Journal of Alloys and Compounds 507 (2010) 489–493

Contents lists available at ScienceDirect

Journal of Alloys and Compounds

journal homepage: www.elsevier.com/locate/jallcom

Hydrogen storage properties of the supersaturated $Mg_{12}YNi$ solid solution

T.Z. Si, Y.F. Liu, Q.A. Zhang*

School of Materials Science and Engineering, Anhui University of Technology, Maanshan, Anhui 243002, PR China

ARTICLE INFO

Article history:
Received 2 July 2010
Received in revised form 26 July 2010
Accepted 27 July 2010
Available online 4 August 2010

Keywords:
Supersaturated solid solution
Melt-spinning
Hydrogenation behavior
Hydrogen storage

ABSTRACT

A supersaturated $Mg_{12}YNi$ solid solution was successfully prepared by melt-spinning technique and its hydrogenation behavior and hydrogen absorption/desorption properties were investigated in detail. It was found that the hydrides of Mg_2Ni and Y are formed accompanying the formation of MgH_2 during the hydrogenation process at 473–573 K. The hydrides of Mg_2Ni and Y have a catalytic effect on the subsequent hydrogen absorption/desorption. Thus, the supersaturated $Mg_{12}YNi$ solid solution has a good activation property and an improved kinetics of hydrogen absorption/desorption.

1. Introduction

Magnesium hydride is considered as a potential hydrogen storage material for vehicular application because of its high capacity and low cost. However, the slow reaction kinetics of the Mg–H_2 system at low temperatures limits its practical application. Hence, numerous attempts, such as doping with catalytic additions [1–5] or/and refining by ball-milling [6–9], have been done to improve the hydrogen absorption/desorption properties of pure Mg. It is well known that alloying with Ni facilitates the diffusion of hydrogen through Mg [8,10] and doping with rare earth elements is beneficial to its hydrogenation properties [11,12]. Thus the joint addition of Ni and rare earth element (La, Ce or Y) is an effective method to improve the hydrogen absorption/desorption properties for the Mg-based alloys [13–16]. For example, the Mg–20 wt.% Ni–Y alloy has good hydrogen absorption/desorption kinetics even at temperature of 523 K [16]. Such a result has attracted more attention in recent years [17–19].

Actually, the hydrogen-induced phase decomposition usually occurs during the hydrogenation processes of Mg–Y–Ni alloys [17–19]. The hydrogenation products, both the hydrides of Mg_2Ni and Y act as catalysts on the hydrogenation/dehydrogenation reactions of the Mg–H_2 system, especially in the case that the refined microstructures are obtained by mechanical alloying (MA) [16] or melt-spinning [18]. It was reported that the melt-spun Mg–Ni–Y alloys with a microstructure of nanocrystalline Mg(Ni,Y) grains embedded in an amorphous matrix have fast hydrogen absorption/desorption kinetics [18]. However, it is uncertain whether all the melt-spun Mg–Ni–Y alloys prepared at various solidification rates have good kinetics of hydrogen absorption/desorption. To clarify this question, we investigate herein the hydrogenation behavior and hydrogen storage properties of the supersaturated $Mg_{12}YNi$ solid solution prepared by melt-spinning with a surface velocity of 20 m/s.

2. Experimental details

The $Mg_{12}YNi$ alloy ingots were prepared by induction melting of appropriate amounts of a mixture of pure Mg (99.9% purity) and an intermediate YNi alloy under an argon atmosphere (about 0.1 MPa). The as-cast alloy was then re-melted and quenched by melt-spinning with a constant rotating copper roller surface velocity of 20 m/s. The continuously long ribbons with width of about 3 mm and thickness of 30–50 μm were obtained. Considering the loss of Mg during induction melting and melt-spinning, extra 18 wt.% of Mg was added to compensate the loss on the basis of stoichiometric composition.

The microstructure characterization of the melt-spun sample was examined using a scanning electron microscope (SEM) XL30 at an accelerating voltage of 20 kV. The SEM sample was first mechanically polished and then etched with 4 mol% nital. To evaluate the phase structures of the melt-spun as well as the de/hydrogenated samples, powder X-ray diffraction (XRD) measurements were carried out on a Rigaku D/Max 2500VL/PC diffractometer with Cu Kα radiation at 50 kV and 200 mA. The XRD profiles were analyzed with the Rietveld refinement program RIETAN-2000 [20].

To investigate the hydrogenation behavior, the powder sample of the melt-spun $Mg_{12}YNi$ alloy was hydrogenated at 473, 523 and 573 K under a hydrogen pressure of 3.0 MPa for 12 h, respectively. The hydrogen absorption/desorption properties were then examined at various temperatures by a Sieverts-type apparatus. The initial hydrogen pressures of hydrogenation and dehydrogenation processes are 3.0 MPa and vacuum, respectively. Before the measurements, the powder samples were activated by three cycles of hydrogen absorption/desorption at 573 K.

* Corresponding author. Tel.: +86 555 2311891; fax: +86 555 2311570.
E-mail address: zhang03jp@yahoo.com.cn (Q.A. Zhang).

0925-8388/$ – see front matter © 2010 Elsevier B.V. All rights reserved.
doi:10.1016/j.jallcom.2010.07.214

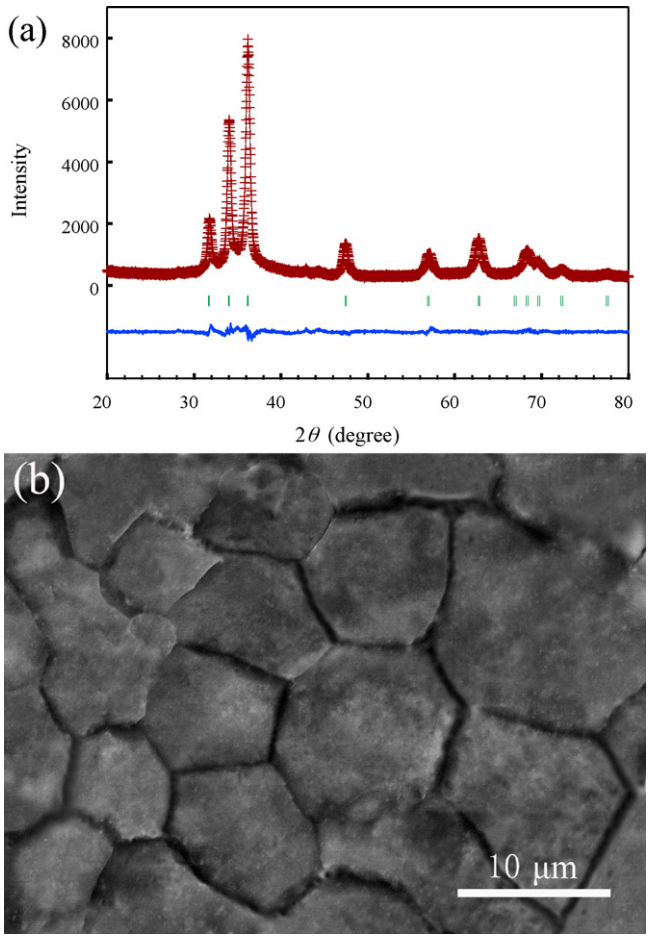

Fig. 1. Calculated (line) and observed (+) X-ray diffraction patterns (a) and SEM image (b) of the melt-spun $Mg_{12}YNi$ sample.

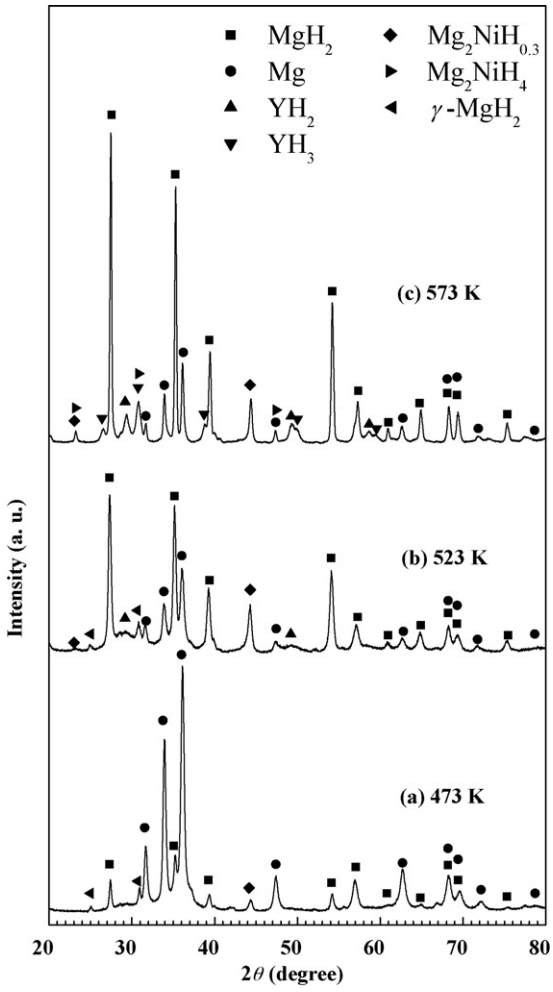

Fig. 2. XRD patterns of the hydrogenated products for the melt-spun $Mg_{12}YNi$ samples.

3. Results and discussion

3.1. Structural characteristics of melt-spun $Mg_{12}YNi$

Fig. 1a shows the Rietveld refinement of the observed XRD pattern for the melt-spun $Mg_{12}YNi$ sample. It can be seen that the sample is composed of a single Mg-based solid solution phase, indicating that the Y and Ni atoms were dissolved in the crystal lattice of Mg. Referring to the Mg–Y and Mg–Ni phase diagrams [21,22], however, one may deduce that the solid solubilities of Y and Ni in Mg are negligible at room temperature. This means the supersaturated $Mg_{12}YNi$ solid solution can be readily prepared under the present condition. The lattice parameters of the supersaturated solid solution were calculated to be $a = 3.2056(7)$ Å and $c = 5.1934(8)$ Å. According to the expression of average atom radius [23,24], the average atom radius of the solid dissolved Y and Ni was calculated to be 1.52 Å. This value is smaller than the atom radius of Mg (1.60 Å) [25], therefore, the lattice parameters of the $Mg_{12}YNi$ solid solution are slightly smaller than those of pure Mg ($a = 3.2125(5)$ Å and $c = 5.2132(8)$ Å [26]).

The microstructure of the melt-spun $Mg_{12}YNi$ sample is shown in Fig. 1b. It can be seen that the average grain size in the sample is about 10 μm. Compared to the melt-spun Mg–Y–Ni alloys with a microstructure of nano-sized grains (about 3 nm) [14], the refinement of grains is unconspicuous in the melt-spun sample under the present conditions. This means that the peak broadening of XRD in Fig. 1a is due to the large lattice strain caused by supersaturation rather than crystallite size. Since synchronous formation of numerous defects and internal strain, the improvement of hydrogen storage properties is expected for the melt-spun $Mg_{12}YNi$.

3.2. Hydrogenation behavior

Fig. 2 shows the XRD patterns of the hydrogenated products for the melt-spun $Mg_{12}YNi$ samples at 473, 523 and 573 K, respectively. It can be seen that the sample hydrogenated at 473 K consists of the main phase Mg and a small amount of $Mg_2NiH_{0.3}$, tetragonal MgH_2 and orthorhombic γ-MgH_2. This indicates that the supersaturated solid solution starts to decompose under a hydrogen pressure of 3.0 MPa at about 473 K. The formation of $Mg_2NiH_{0.3}$ is coincident with the fact that the crystallization of Mg_2Ni occurred from the amorphous Mg–Ni–Y alloys under argon atmosphere at 473 K [18]. The appearance of the metastable γ-MgH_2 is likely to be related to the high internal stress in the supersaturated solid solution [27].

The Rietveld analysis result for the sample hydrogenated at 523 K is shown in Fig. 3 as a representative example of the hydrogenated $Mg_{12}YNi$ samples. Obviously, the diffraction pattern calculated from the structure models is in good agreement with that measured. The structural parameters and phase abundance of the hydrogenated products calculated by the XRD Rietveld analysis are listed in Table 1. It can be seen that the abundance of the MgH_2 (including both tetragonal and orthorhombic MgH_2) markedly increases from 13 to 64 wt.% with increasing the hydrogenation temperature from 473 to 523 K. Besides 12 wt.% of $Mg_2NiH_{0.3}$, it is interesting that the YH_2 is also formed in the hydrogenated sample.

Table 1
Structural parameters and phase abundance of the hydrogenated products for the melt-spun $Mg_{12}YNi$ samples.

Hydrogenated sample	Phase	Space group	R_I (%)	Lattice parameters			Abundance (wt.%)
				a (Å)	b (Å)	c (Å)	
At 473 K	MgH_2	$P4_2/mnm$	2.72	4.5091(2)		3.0172(1)	10
R_{wp} = 5.92%	Mg	$P6_3/mmc$	2.14	3.2053(2)		5.1963(2)	84
S = 1.43	$Mg_2NiH_{0.3}$	$P6_222$	2.72	5.1427(8)		14.174(2)	3
	γ-MgH_2	Pbcn	2.25	4.5234(4)	5.4532(5)	4.9525(4)	3
At 523 K	MgH_2	$P4_2/mnm$	0.55	4.5119(9)		3.0169(7)	56
R_{wp} = 6.40%	Mg	$P6_3/mmc$	0.63	3.2046(9)		5.1924(1)	19
S = 1.74	YH_2	Fm-3m	0.82	5.1837(3)			5
	γ-MgH_2	Pbcn	0.65	4.5216(4)	5.4435(3)	4.9467(4)	8
	$Mg_2NiH_{0.3}$	$P6_222$	0.85	5.2291(2)		13.345(5)	12
At 573 K	MgH_2	$P4_2/mnm$	2.43	4.5147(2)		3.0203(1)	69
R_{wp} = 7.42%	Mg	$P6_3/mmc$	2.80	3.2124(4)		5.2125(5)	11
S = 2.22	YH_2	Fm-3m	3.22	5.1854(1)			4
	YH_3	$P6_3/mmc$	3.12	3.6631(9)		6.6063(5)	5
	$Mg_2NiH_{0.3}$	$P6_222$	2.65	5.2332(1)		13.349(3)	8
	Mg_2NiH_4	Cm	3.41	6.4314(7)	5.9889(1)	6.9566(2)	3

A more complete hydrogenation reaction can be obtained at 573 K, as shown in Fig. 2c and Table 1. Besides 69 wt.% of MgH_2, the sample contains a small amount of Mg, YH_2, YH_3, $Mg_2NiH_{0.3}$ and Mg_2NiH_4. To our knowledge, Mg_2Ni can be hydrogenated to form Mg_2NiH_4 about at 523 K. However, 8 wt.% of $Mg_2NiH_{0.3}$ still remains in the sample hydrogenated at 573 K, which is analogous to the phenomenon occurred in the amorphous $Mg_{90}Y_5Ni_5$ sample hydrogenated at 623 K [18], though the actual reason is unknown yet. In a word, the hydrides of Mg_2Ni and Y are formed accompanying the formation of MgH_2 during the hydrogenation process, which is the typical feature of the hydrogenation behavior of the supersaturated $Mg_{12}YNi$ solid solution.

3.3. Hydrogen absorption/desorption properties

Fig. 4 shows the cyclic curves of hydrogen absorption/desorption of the supersaturated $Mg_{12}YNi$ solid solution at 573 K. It can be seen that the sample is easy to be activated within 3 cycles. After 3 cycles, the hydrogen absorption and desorption contents reach up to 4.74 and 4.62 wt.%, respectively. This means that the supersaturated solid solution has a good activation property at 573 K, which is comparable with that of the melt-spun Mg–Y–Ni alloys with a microstructure of nanocrystalline Mg(Ni,Y) grains embedded in an amorphous matrix [18]. The improved activation property is actually related to Mg_2Ni and the hydrides of Y. Fig. 5 shows the XRD pattern of the sample after three cycles of hydrogen absorption/desorption at 573 K. Obviously, Mg_2Ni, YH_2 and YH_3 are present together with Mg in the dehydrogenated sample. Furthermore, these phases are also favorable to the kinetics of hydrogen absorption/desorption, which will be discussed below.

It is well known that the hydrogen absorption and desorption of pure Mg are kinetically slow at 573 K. However, this shortcoming has been greatly overcome for the melt-spun $Mg_{12}YNi$ alloy.

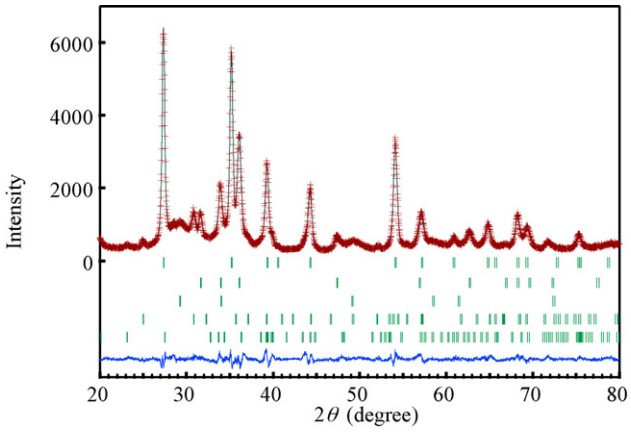

Fig. 3. Calculated (line) and observed (+) X-ray diffraction patterns of the hydrogenated products for the melt-spun $Mg_{12}YNi$ sample at 523 K (vertical bars below the patterns show the positions of all possible reflection peaks of the MgH_2, Mg, YH_2, γ-MgH_2 and $Mg_2NiH_{0.3}$ phases).

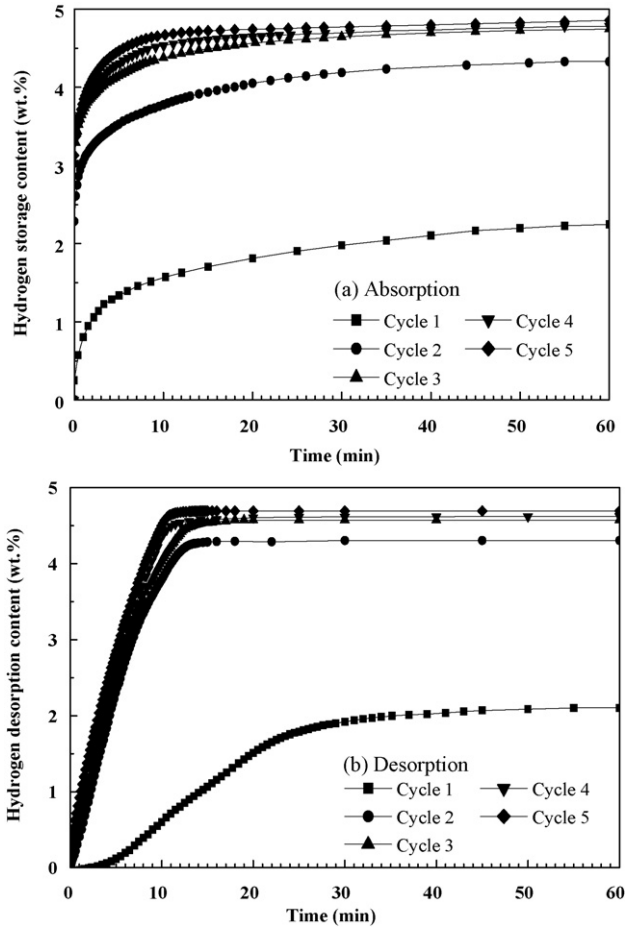

Fig. 4. Cyclic curves of hydrogen absorption/desorption of the melt-spun $Mg_{12}YNi$ sample at 573 K.

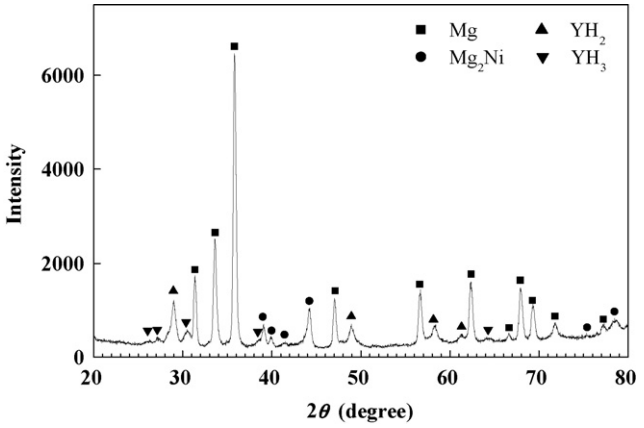

Fig. 5. XRD pattern of the $Mg_{12}YNi$ sample after three cycles of hydrogen absorption/desorption at 573 K.

The kinetic curves of hydrogen absorption of the activated $Mg_{12}YNi$ sample are shown in Fig. 6. It can be seen that the sample can absorb 3.56, 4.12 and 4.3 wt.% hydrogen within 5 min at 473, 523 and 573 K, respectively. In comparison with the 2.6 wt.% of hydrogen absorption content within 300 min at 473 K for the as-cast Mg–Y–Ni [15], the kinetics of hydrogen absorption of the melt-spun $Mg_{12}YNi$ sample is improved remarkably. It is notable that the initial hydrogen absorption rate can reach 0.82 wt.%-H/min at 523 K, which is slightly slower than that of the melt-spun Mg–Y–Ni alloys with a microstructure of nanocrystalline Mg(Ni,Y) grains embedded in an amorphous matrix obtained at a surface velocity of 40 m/s [18]. Fig. 7 shows the kinetic curves of hydrogen desorption of the activated $Mg_{12}YNi$ sample. It can be seen that this sample can desorb 4.12 wt.% hydrogen within 60 min at 523 K. The kinetics of hydrogen desorption at 523 K is faster than that of the milled MgH_2 [28] but also slower than that of the melt-spun Mg–Y–Ni alloys prepared with a surface velocity of 40 m/s [18].

Based on the experimental results above, it is evident that the supersaturated $Mg_{12}YNi$ solid solution prepared by melt-spinning with a surface velocity of 20 m/s has a faster kinetics of hydrogen absorption/desorption than the ball-milled MgH_2 without catalyst [28]. However, the kinetics of hydrogen absorption/desorption is slower than that of the melt-spun Mg–Y–Ni alloys with a microstructure of nanocrystalline Mg(Ni,Y) grains embedded in an amorphous matrix obtained at a surface velocity of 40 m/s [18]. This means that both the nano-sized effect of Mg(Ni,Y) grains and

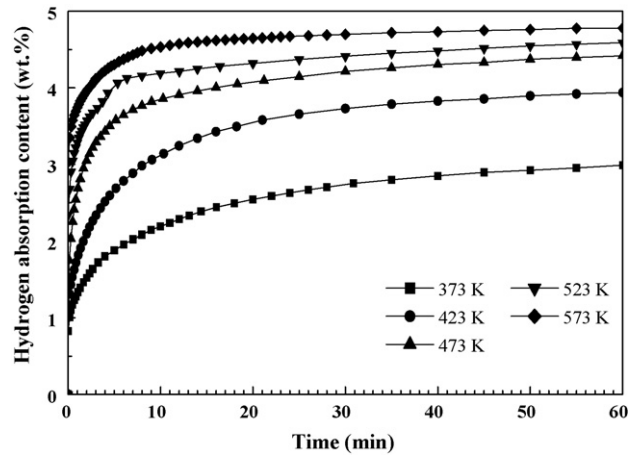

Fig. 6. Kinetic curves of hydrogen absorption of the activated $Mg_{12}YNi$ sample under an initial hydrogen pressure of 3.0 MPa.

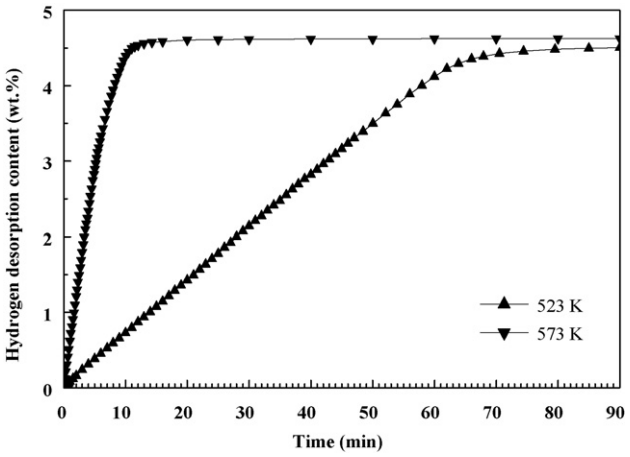

Fig. 7. Kinetic curves of hydrogen desorption of the activated $Mg_{12}YNi$ sample under an initial state of vacuum.

the catalytic effect of the hydrides of Mg_2Ni and Y are favorable to the kinetics of hydrogen absorption/desorption. Thus, it is necessary to increase solidification rate for obtaining a nano-sized microstructure in Mg–Y–Ni alloys. The optimum solidification rate is interesting and important for developing $Mg_{12}YNi$ hydrogen storage alloy. Thus, the more detailed investigation is in process.

4. Conclusions

The hydrogenation behavior and hydrogen absorption/desorption properties of the supersaturated $Mg_{12}YNi$ solid solution prepared by melt-spinning were investigated in this paper. It was found that the hydrides of Mg_2Ni and Y are formed accompanying the formation of MgH_2 during the hydrogenation process at 473–573 K. The hydrides of Mg_2Ni and Y have a catalytic effect on the subsequent hydrogen absorption/desorption. Thus the supersaturated $Mg_{12}YNi$ solid solution can be activated easily within three cycles of hydrogen absorption/desorption at 573 K and the activated $Mg_{12}YNi$ sample has a faster kinetics of hydrogen absorption/desorption. However, it is necessary to further improve the kinetic property by refining microstructures.

Acknowledgements

This work was financially supported by the National Natural Science Foundation of China (Nos. 50771001 and 50971001).

References

[1] H.B. Lu, C.K. Poh, L.C. Zhang, et al., J. Alloys Compd. 481 (2009) 152.
[2] L.P. Ma, P. Wang, H.M. Cheng, J. Alloys Compd. 432 (2007) L1.
[3] M. Tanniru, F. Ebrahimi, Int. J. Hydrogen Energy 34 (2009) 7714.
[4] V. Fuster, G. Urretavizcaya, F.J. Castro, J. Alloys Compd. 481 (2009) 673.
[5] M.Y. Song, S.N. Kwon, J.S. Bae, S.H. Hong, J. Alloys Compd. 478 (2009) 501.
[6] Z.L. Lei, Z.Y. Liu, Y.B. Chen, J. Alloys Compd. 470 (2009) 470.
[7] T. Spassov, P. Delchev, P. Madjarov, et al., J. Alloys Compd. 495 (2010) 149.
[8] G. Liang, S. Boily, J. Huot, A. Van Neste, R. Schulz, J. Alloys Compd. 267 (1998) 302.
[9] G. Liang, J. Huot, S. Boily, R. Schulz, J. Alloys Compd. 305 (2000) 239.
[10] D. Vojtech, P. Guhlova, M. Mortanikova, P. Janik, J. Alloys Compd. 494 (2010) 456.
[11] C. Zlotea, M. Sahlberg, P. Moretto, Y. Andersson, J. Alloys Compd. 489 (2010) 375.
[12] Y.H. Zhang, D.L. Zhao, S.H. Guo, et al., J. Alloys Compd. 476 (2009) 457.
[13] Y. Wu, M.V. Lototsky, J.K. Solberg, et al., J. Alloys Compd. 477 (2009) 262.
[14] T. Spassov, V. Rangelova, N. Neykov, J. Alloys Compd. 334 (2002) 219.
[15] M. Hara, S. Morozumi, K. Watanabe, J. Alloys Compd. 414 (2006) 207.
[16] Z.N. Li, X.P. Liu, L.J. Jiang, S.M. Wang, Int. J. Hydrogen Energy 32 (2007) 1869.
[17] A. Gebert, B. Khorkounov, U. Wolff, et al., J. Alloys Compd. 419 (2006) 319.
[18] S. Kalinichenka, L. Rontzsch, B. Kieback, Int. J. Hydrogen Energy 34 (2009) 7749.
[19] K. Tanaka, T. Miwa, K. Sasaki, K. Kuroda, J. Alloys Compd. 478 (2009) 308.

[20] F. Izumi, T. Ikeda, Mater. Sci. Forum 321–323 (2000) 198.
[21] A.A. Nayeb-Hashemi, J.B. Clark, Phase Diagrams of Binary Magnesium Alloys, ASM International, Metals Park, OH, 1988, p. 344.
[22] K.H.J. Buschow, Solid State Commun. 17 (1975) 891.
[23] N. Terashita, K. Kobayashi, E. Akiba, J. Alloys Compd. 327 (2001) 275.
[24] Q.A. Zhang, E. Akiba, H. Enoki, J. Alloys Compd. 322 (2001) 257.
[25] J. Zhang, G.Y. Zhou, G. Chen, et al., Acta Mater. 56 (2008) 5388.
[26] P. Karen, A. Kjekshus, Q. Huang, V.L. Karen, J. Alloys Compd. 282 (1999) 72.
[27] J.P. Bastide, B. Bonnetot, J.M. Letoffe, P. Claudy, Mater. Res. Bull. 15 (1980) 1215.
[28] G. Liang, J. Huot, S. Boily, A. Van Neste, R. Schulz, J. Alloys Compd. 292 (1999) 247.